Report

# MODELING GLOW DISCHARGES: What Can We Learn from It?

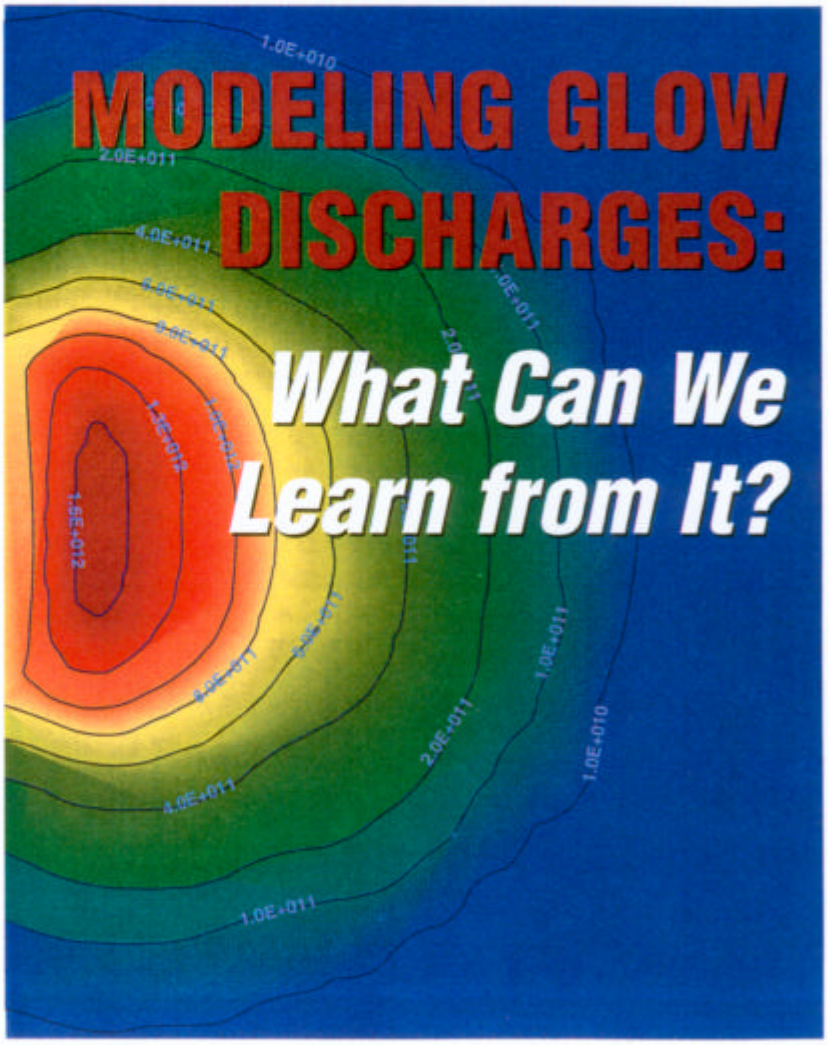


*Mathematical modeling of GDs is useful for obtaining information that is experimentally hard to acquire.*

Plasma sources, such as inductively coupled plasmas (ICPs), microwave-induced plasmas, and glow discharges (GDs), are attracting increasing interest as atomization/excitation/ionization sources in atomic spectrometry. A clear understanding of the fundamental processes taking place in the GD plasma is thus desirable and can be obtained by plasma diagnostic experiments (measuring characteristic plasma quantities) or by mathematical modeling of the plasma (simulation of the behavior of the various plasma species). In practice, some plasma quantities are difficult to measure because the GD extends only into a small region and plasma diagnostic experiments often disturb the real plasma. Therefore, mathematical modeling is sometimes useful for obtaining information that is experimentally hard to acquire. In this Report, we present state-of-the-art modeling of analytical GDs and show some typical examples of what can be calculated with such models.

## A brief explanation

The basics of a GD and its analytical applications have been previously described in *Analytical Chemistry* (*1*, *2*); therefore, an abbreviated explanation of the working principles is presented. A GD is a partially ionized gas, or plasma, consisting of nearly equal concentrations of positive and negative charges, plus a large number of neutral species. In its simplest form, it can be created by inserting two electrodes

**Annemie Bogaerts**
**Renaat Gijbels**
*University of Antwerp (Belgium)*

into a cell filled with gas at low pressure (e.g., Ar at ~1 mbar). Between the two electrodes, a voltage of ~1 kV is applied. The analytical GD can be spatially divided into three regions: the cathode dark space (CDS) close to the cathode, which is characterized by a high electric field (the entire potential applied between the two electrodes drops off in this region); the negative glow (NG), which is nearly field-free and fills up most of the discharge region; and a small anode dark space (ADS) adjacent to the anode.

The potential applied between the two electrodes causes electrical breakdown of the gas, that is, the formation of positive ions and electrons. The positive ions are accelerated toward the cathode by the electric field in front of it, in the CDS. Ion bombardment of the cathode causes the release of secondary electrons, which are accelerated away from the cathode. When the electrons arrive in the GD plasma, they can produce ionization and excitation collisions with the gas particles.

The excitation and subsequent radiative decay processes, with the emission of light, are responsible for the characteristic "glow". The ionization collisions give rise to new electron–ion pairs; the electrons can

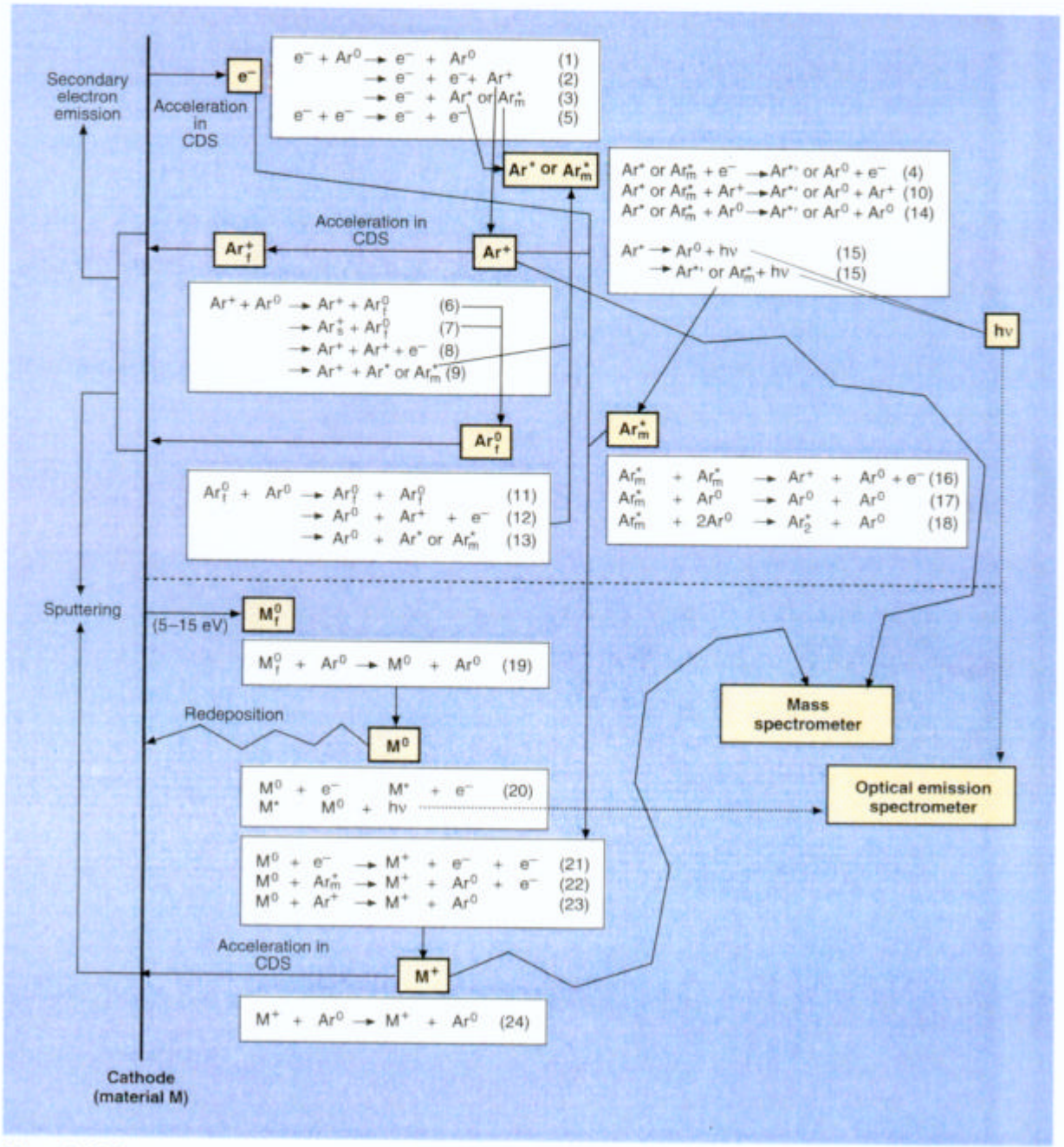


**Figure 1. Main processes occurring in a dc GD in Ar.**

be accelerated again and produce additional ionization, whereas the ions are again accelerated toward the cathode, yielding secondary electron emission. These processes make the GD a self-sustaining plasma. Figure 1 is a schematic of the main processes occurring in a dc GD using Ar.

The use of a GD as the analytical source for MS and optical spectrometric techniques is based on the phenomenon of sputtering. The material to be analyzed is used as the cathode of the GD. The ions from the plasma and fast atoms (i.e., atoms with energies >0.05 eV created by ion collisions) release electrons when they bombard the cathode and give rise to the ejection of atoms of the cathode material, which is called sputtering. The sputtered cathode atoms arrive in the plasma, where they can be ionized or excited. The ions created in this way can be separated and detected in the mass spectrometer. The characteristic photons, produced by the excitation and radiative deexcitation processes, can be used for GD-optical emission spectrometry. The sputtered atoms in the plasma can also be probed by an external light source, making GD-atomic absorption and GD-atomic fluorescence spectrometries possible. Moreover, the GD can be used in hybrid analytical constructions in combination with lasers, graphite furnaces, secondary discharges, or magnetic fields (*1–3*).

## Different modeling approaches

GDs are also extensively used for depositing thin layers, plasma etching, and modifying surfaces, as well as plasma displays, light sources, and metal-vapor ion lasers (*4*). Modeling of these GDs, which operate under slightly different conditions, has been reported in the plasma physics literature during the past few decades. The processes occurring in analytical and other types of GDs are quite similar, so that the basics of the models that we have developed for analytical GDs could be deduced from existing models in the plasma physics literature. However, these models had to be modified and extended to other plasma species, because analytical scientists are interested in the behavior of the sputtered species, whereas plasma physicists focus their attention on the electrical characteristics of the GD. Moreover, because analytical GDs operate under different discharge

**Table 1. Collision processes in the plasma incorporated in the models. (The most important processes are shown in Figure 1.)**

| | |
|---|---|
| (1) Electrons: elastic collisions with Ar atoms | $e^- + Ar^0 \rightarrow e^- + Ar^0$ |
| (2) Electrons: ionization of Ar ground-state atoms (or excited or metastable atoms) | $e^- + Ar^0 \rightarrow e^- + Ar^+ + e^-$<br>$(e^- + Ar^* \text{ or } Ar^*_m \rightarrow e^- + e^- + Ar^+)$ |
| (3) Electrons: excitation of Ar ground-state atoms (or excited or metastable atoms) | $e^- + Ar^0 \rightarrow e^- + Ar^* \text{ or } Ar^*_m$<br>$(e^- + Ar^* \text{ or } Ar^*_m \rightarrow e^- + Ar^{*'})$ |
| (4) Electrons: deexcitation of excited Ar levels (including metastable levels) | $e^- + Ar^* \text{ or } Ar^*_m \rightarrow e^- + Ar^{*'} \text{ or } Ar^0$ |
| (5) Electrons: coulomb scattering with other electrons | $e^- + e^- \rightarrow e^- + e^-$ |
| (6) Ar ions: elastic collisions with Ar atoms | $Ar^+ + Ar^0 \rightarrow Ar^+ + Ar^0_f$ |
| (7) Ar ions: symmetric charge-transfer collisions with Ar atoms | $Ar^+ + Ar^0 \rightarrow Ar^0_f + Ar^+_s$ |
| (8) Ar ions: ionization of Ar ground-state atoms (or excited or metastable atoms) | $Ar^+ + Ar^0 \rightarrow Ar^+ + Ar^+ + e^-$<br>$(Ar^+ + Ar^* \text{ or } Ar^*_m \rightarrow Ar^+ + Ar^+ + e^-)$ |
| (9) Ar ions: excitation of Ar ground-state atoms (or excited or metastable atoms) | $Ar^+ + Ar^0 \rightarrow Ar^+ + Ar^* \text{ or } Ar^*_m$<br>$(Ar^+ + Ar^* \text{ or } Ar^*_m \rightarrow Ar^+ + Ar^{*'})$ |
| (10) Ar ions: deexcitation of excited Ar levels (including metastable levels) | $Ar^+ + Ar^* \text{ or } Ar^*_m \rightarrow Ar^+ + Ar^{*'} \text{ or } Ar^0$ |
| (11) Fast Ar atoms: elastic collisions with Ar atoms | $Ar^0_f + Ar^0 \rightarrow Ar^0_f + Ar^0_f$ |
| (12) Fast Ar atoms: ionization of Ar ground-state atoms (or excited or metastable atoms) | $Ar^0_f + Ar^0 \rightarrow Ar^0 + Ar^+ + e^-$<br>$(Ar^0_f + Ar^* \text{ or } Ar^*_m \rightarrow Ar^0 + Ar^+ + e^-)$ |
| (13) Fast Ar atoms: excitation of Ar ground-state atoms (or excited or metastable atoms) | $Ar^0_f + Ar^0 \rightarrow Ar^0 + Ar^* \text{ or } Ar^*_m$<br>$(Ar^0_f + Ar^* \text{ or } Ar^*_m \rightarrow Ar^0 + Ar^{*'})$ |
| (14) Fast Ar atoms: deexcitation of excited Ar levels (including metastable levels) | $Ar^0 + Ar^* \text{ or } Ar^*_m \rightarrow Ar^0 + Ar^{*'} \text{ or } Ar^0$ |
| Electron–Ar ion radiative recombination | $e^- + Ar^+ \rightarrow Ar^0 \text{ or } Ar^* \text{ or } Ar^*_m + h\nu$ |
| Electron–Ar ion three-body recombination in which the third body is an electron | $e^- + Ar^+ + e^- \rightarrow Ar^0 \text{ or } Ar^* \text{ or } Ar^*_m + e^-$ |
| Electron–Ar ion three-body recombination in which the third body is an Ar ion | $e^- + Ar^+ + Ar^+ \rightarrow Ar^0 \text{ or } Ar^* \text{ or } Ar^*_m + Ar^+$ |
| Electron–Ar ion three-body recombination in which the third body is an Ar atom | $e^- + Ar^+ + Ar^0 \rightarrow Ar^0 \text{ or } Ar^* \text{ or } Ar^*_m + Ar^0$ |
| (15) Radiative decay of excited Ar levels | $Ar^* \rightarrow Ar^0 \text{ or } Ar^{*'} \text{ or } Ar^*_m + h\nu$ |
| (16) Ar metastable atom–metastable atom collisions | $Ar^*_m + Ar^*_m \rightarrow Ar^+ + Ar^0 + e^-$ |
| (17) Two-body collisions of Ar metastable atoms with Ar atoms | $Ar^*_m + Ar^0 \rightarrow Ar^0 + Ar^0$ |
| (18) Three-body collisions of Ar metastable atoms with Ar atoms | $Ar^*_m + 2Ar^0 \rightarrow Ar^*_2 + Ar^0$ |
| (19) M (sputtered) atoms: elastic collisions with Ar atoms → until thermalized | $M^0_f + Ar^0 \rightarrow M^0 + Ar^0$ |
| (20) M atoms: electron excitation followed by radiative decay | $e^- + M^0 \rightarrow e^- + M^*$<br>$M^* \rightarrow M^0 + h\nu$ |
| (21) M atoms: electron-impact ionization | $e^- + M^0 \rightarrow e^- + M^+ + e^-$ |
| (22) M atoms: Penning ionization by Ar meta-stable atoms | $Ar^*_m + M^0 \rightarrow Ar^0 + M^+ + e^-$ |
| (23) M atoms: asymmetric charge transfer with Ar ions | $Ar^+ + M^0 \rightarrow Ar^0 + M^+$ |
| (24) M ions: elastic collisions with Ar atoms | $M^+ + Ar^0 \rightarrow M^+ + Ar^0$ |

The symbols $e^-$, $Ar^+$, $Ar^0$, $Ar^*$, and $Ar^*_m$ denote electrons, singly charged Ar ions, Ar ground-state atoms, excited Ar atoms, and Ar metastable atoms, respectively. $Ar^{*'}$ means Ar atoms in another excited level. $M^0$ and $M^+$ are sputtered cathode atoms and the corresponding ions, and the subscripts f and s indicate fast and slow atoms or ions, respectively. The cross sections for all these processes, as a function of the colliding particles' energies, are adopted from the literature. The processes in parentheses are of lesser importance in the plasma.

**Table 2. Models used to describe various plasma species.**

| Plasma species | Model | References |
|---|---|---|
| Fast electrons | MC (entire discharge) | 12, 13, 18 |
| Thermalized electrons | Fluid (entire discharge) | 13, 18 |
| Ar ions | Fluid (entire discharge)<br>MC (CDS) | 13, 18<br>12, 14 |
| Fast Ar atoms | MC (CDS) | 12, 14 |
| Ar metastable atoms | Fluid (entire discharge) | 15, 19 |
| Various excited Ar levels | Fluid (collisional radiative model; entire discharge) | 21 |
| Cathode atoms: thermalization process | MC (entire discharge) | 16 |
| Cathode atoms + ions: transport + ionization | Fluid (entire discharge) | 17, 19 |
| Cathode ions | MC (CDS) | 17, 19 |

conditions, it can be expected that other plasma processes come into play.

There are three basic groups of models to describe GDs reported in the plasma physics literature. In a fluid model (*5–7*), the plasma species (electrons, atoms, and ions) are considered to be a continuum in equilibrium with the electric field and are described by continuity equations (based on conservation laws) and flux equations of diffusion and migration in the electric field (the latter only for charged particles). This kind of modeling is, in principle, quite simple (although it can be tricky to solve a set of strongly coupled nonlinear differential equations), but it is only an approximation—especially for the electrons, which are definitely not in equilibrium with the electric field (they gain more energy from the electric field than they lose by collisions).

The second approach is a Boltzmann model (*8, 9*) that copes with nonequilibrium of the various plasma species by describing them with Boltzmann transport equations. This method is accurate but can lead to very complex mathematical equations. The third model is Monte Carlo (MC) simulation (*10, 11*). The behavior of the species is simulated explicitly; they are described as separate particles, one after the other. Their trajectories throughout the discharge is described by Newton's laws, and collisions are treated with random numbers. (The probability of a certain collision process and the new energy and direction after a collision are defined based on cross sections and scattering theories using randomly created numbers.) By following a large number of particles, the GD can be simulated. This model is the most accurate one, because it deals with the particles on the lowest microscopical level. Moreover, it is based on rather simple equations, making it transparent and easy to understand. However, because a large number of particles are followed for simulation (which allows satisfactory statistics to be obtained), calculation times are long for slow-moving particles.

*A combination of models can be used to describe the various species in the GD.*

Hence, each model has its advantages and disadvantages, and it is therefore desirable to use a combination of these models to describe the various species in the GD. Species that are not in equilibrium with the electric field, such as fast electrons (electrons with a high enough energy to produce ionization or excitation), must be treated with an MC model, whereas species that are more or less in equilibrium with the electric field can be described sufficiently accurately with a fluid model.

## Modeling an analytical GD

In the past few years, we have developed a comprehensive modeling network for an analytical dc GD using Ar (*12–21*). The different species assumed to be present in the plasma and described in the models are Ar gas atoms at rest, uniformly distributed throughout the discharge; electrons, subdivided into a fast and a thermalized group; singly charged Ar ions; fast Ar atoms created from Ar ions by symmetric charge transfer and elastic collisions (Table 1); Ar atoms in various excited levels with special emphasis on the metastable levels (levels that cannot decay radiatively to lower levels and have a longer lifetime; these so-called "metastable atoms" play an important role in the GD by Penning ionization of the sputtered atoms) (Table 1); and atoms and ions of the cathode material to be analyzed. Molecular species, such as argides, are not considered.

The species are described with a combination of fluid approaches and MC simulations (Table 2). The MC models are developed completely in three dimensions. Because of the nearly cylindrical symmetry of the discharge cells to which the models are applied, the 3-D fluid models could be reduced to 2-D calculations using axial and radial directions (*12–21*). The various collision processes taking place in the plasma and incorporated into the models are schematically indicated in Figure 1. The numbers after each process correspond to those in Table 1. Most processes occur throughout the entire GD plasma, but the collisions of Ar ions and fast Ar atoms take place only in the CDS. Only the main processes are indicated in Figure 1; the reality is probably much more complicated. For example, ion–electron recombination is not included in the figure because it is of minor importance in the GD plasma; it takes place mainly at the cell walls.

To describe all these processes, an accurate set of cross sections, as a function of the colliding particles' energies, is required. Other input data needed are diffusion and mobility coefficients, as well as data related to the processes occurring at the cell walls (i.e., a secondary electron emission coefficient and sticking coefficients of the plasma species) and data necessary to calculate the cathode sputtering.

The different models are all coupled to each other because of the interaction processes between the plasma species, and they are solved iteratively until final convergence is reached, to obtain an overall

picture of the GD (*18–20*). Figure 2 is a flowchart that illustrates the various links between the models. A complete "run" of the modeling network takes about a week on a workstation with 128-MB memory and four coprocessors, each with 50-MHz clock speed.

## Typical results

Table 3 (*12–33*) presents an overview of typical results obtained with the models. All these plasma quantities can be calculated for different discharge conditions and cell geometries. The effects of discharge conditions (voltage, current, pressure), cell dimensions, and cell geometry (e.g., cells with pin and flat cathodes) have been investigated (*20, 25, 26*). To test the validity of the models, the calculated quantities must be compared with experimental data. Such a comparison has already been carried out for some quantities (indicated in Table 3); in general, reasonable agreement between experimental and modeling results was obtained.

Some of the other calculated quantities presented in Table 3 can, in principle, also be measured (e.g., Stark measurements for obtaining the electric field distribution). However, we are not aware of such experiments performed in similar cells and under similar discharge conditions to assume in our models, so direct comparison with our calculated results is not yet possible.

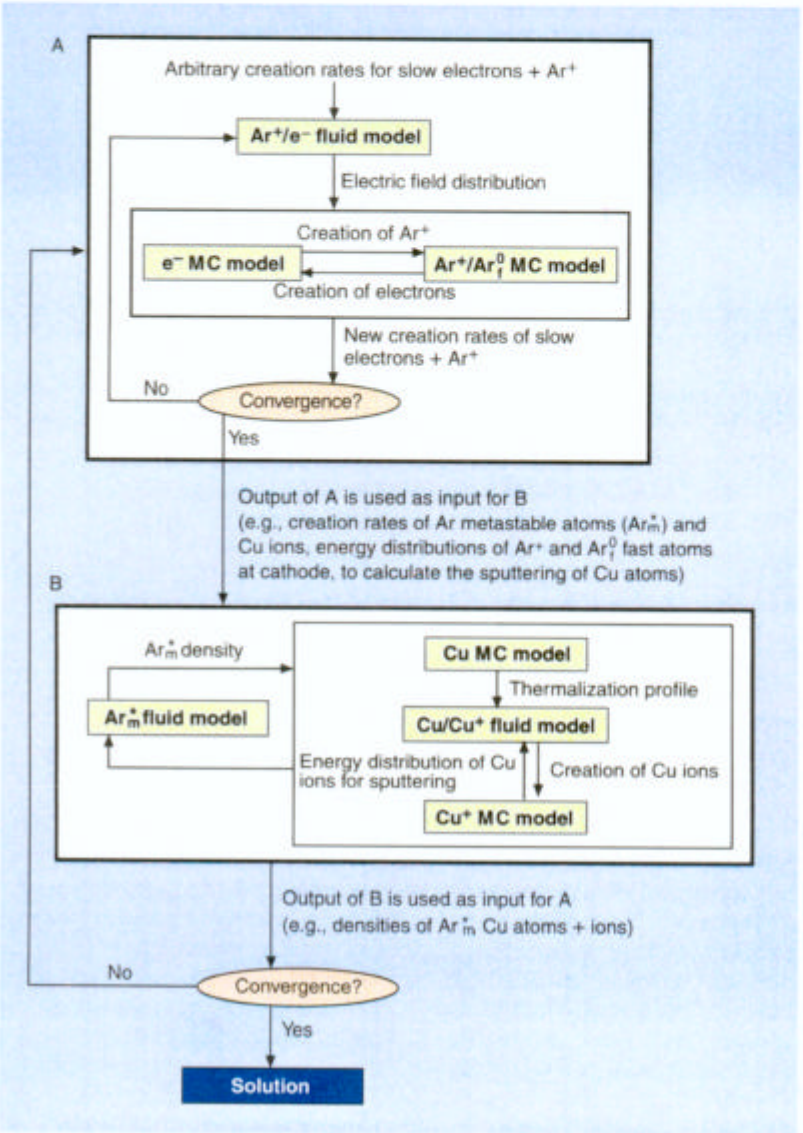


**Figure 2. Flowchart of the combination of the various models.**

Some of the characteristic calculated plasma quantities are illustrated in Figure 3 and are typical for an ~1-cm analytical GD cell consisting of CDS, NG, and ADS regions. They were calculated at typical discharge conditions used in GDMS. The potential and electric field distributions are shown in Figure 3a. The potential (left axis) is –1000 V at the cathode and increases to zero at ~0.23 cm from the cathode. The position where the potential crosses the zero line is defined as the interface between the CDS and NG. The potential is slightly positive in the NG (i.e., by a few volts, known as the plasma potential) and decreases to zero at the anode. Hence, the NG plasma is the most positive part of the discharge. The electric field (right axis) is extremely negative at the cathode (–8 kV/cm) and increases almost linearly in the CDS. It does not cross the zero-line at the CDS–NG interface but bends off to a small negative value in the NG. It goes through zero at about 0.7 cm and then takes on small positive values. Close to the anode, in the ADS, it rises to about 200 V/cm.

Figures 3b and 3c present the density profiles of the various plasma species. In Figure 3b, the Ar metastable atom density (left axis) reaches a maximum of about $10^{12}$ $cm^{-3}$ rather close to the cathode and decreases to small values in the rest of the discharge. The Ar ion density (left axis) is small and more or less constant in the CDS and reaches a broad maximum of $5 \times 10^{11}$ $cm^{-3}$, after which it decreases to a low value at the anode. The slow electron number density (left axis) is zero in the CDS and ADS, and it is almost equal to the Ar ion density in the NG. This gives rise to a net positive space charge in the CDS and ADS, and to an almost neutral charge in the NG. The latter defines the characteristic potential and electric field distributions presented in Figure 3a. The fast electron number density in Figure 3b (right axis) reaches a maximum in the beginning of the NG; it is, however, 4 orders of magnitude lower than the Ar ion and slow electron densities and does not contribute to the space charge.

The sputtered Cu atom density in Figure 3c (left axis) is at its maximum ($\sim 6 \times 10^{12}$ $cm^{-3}$) close to the cathode and decreases almost linearly toward the

**Table 3. Quantities that have been calculated with the models compared with experimental data.**

| Calculated quantities | References | Experimental data | References |
|---|---|---|---|
| Electrical current (function of voltage and pressure) | 14, 20 | Measured with GDMS | 14, 20 |
| 3-D Potential distributions | 13, 18, 20 | NA | |
| 3-D Axial and radial electric field distributions | 13, 18, 20 | NA | |
| Plasma potential | 13, 18, 20 | NA | |
| Length of CDS, NG, ADS | 13, 18, 20 | Length of CDS as function of pressure and current | 22 |
| 3-D Density profiles of | | | |
| Ar ions | 13, 18, 20 | NA | |
| fast Ar atoms | 12, 20 | NA | |
| Ar metastable atoms | 15, 19–21 | Measured by LIF | 23 |
| other excited Ar levels | 21 | NA | |
| fast electrons | 12, 13, 18, 20 | NA | |
| thermalized electrons | 13, 18, 20 | NA | |
| atoms of the cathode material | 17, 19, 20 | Measured by LIF | 24 |
| ions of the cathode material | 17, 19, 20 | Measured by LIF | 24 |
| Ion fluxes of Ar and cathode ions at the exit slit of the cell to the mass spectrometer | 25, 26 | Ratio is in qualitative agreement with ratios in the mass spectra of GDMS | 25 |
| Ionization degrees of Ar and cathode atoms | 17, 19, 20 | Based on LIF results from above | 24 |
| 3-D Energy distributions and mean energies of | | | |
| electrons | 12, 13, 20 | NA | |
| Ar ions | 12, 20 | Measured at the cathode with GDMS | 27 |
| fast Ar atoms | 12, 20 | NA | |
| cathode ions | 17, 20 | Measured at the cathode with GDMS | 27 |
| 3-D Collision rates of electrons, Ar ions, fast Ar atoms, and importance of these processes | 12–14, 18, 20 | NA | |
| 3-D Rates of Penning ionization, asymmetric charge transfer and electron impact ionization, and relative contributions to the total ionization of sputtered atoms | 17, 19, 20 | NA | |
| 3-D Rates and contributions of populating and depopulating processes of metastable and other excited Ar levels | 15, 19–21 | NA | |
| Sputtering rates at the cathode | 17, 19, 20, 28 | Values measured for GDMS | 29 |
| Thermalization profiles of sputtered atoms | 16, 20 | NA | |
| Amount of redeposition on the cathode by backscattering or backdiffusion | 16, 20, 28 | NA | |
| Contributions of Ar ions, fast Ar atoms, and cathode ions to the sputtering process | 12, 17, 19, 20 | NA | |
| 2-D Crater profiles caused by sputtering at the cathode | 28 | Profiles obtained by GDMS | 29 |
| Emission spectra and profiles caused by radiative decay from excited levels | 21 | Data from literature | 30, 31 |
| Prediction of variations in RSFs for GDMS | 32 | Data from literature | 33 |

NA = Not available
LIF = Laser-induced fluorescence
RSF = Relative sensitivity factor

anode. The Cu ion density (right axis) shows the same profile shape as the Ar ion density but is about 2 orders of magnitude lower. It can also be deduced that the ionization degree of sputtered Cu atoms (i.e., the ratio of Cu ion to Cu atom density) is ~0.1%. This calculated value should not be considered too strictly because it depends strongly on the discharge conditions, cell geometry, and type of cathode material; for other conditions, values on the order of a few percent were calculated.

The fluxes of the dominant current carriers are indicated in Figure 3d. In the CDS, most current is carried by the Ar ions, which are directed toward the cathode by the strong electric field in front of it. The fast electron flux at the cathode is about an order of magnitude lower than the Ar ion flux (determined by the ion-induced secondary electron emission coefficient, which is ~0.1), and it is in the opposite direction (i.e., away from the cathode). It increases in the CDS and remains nearly constant in the NG. The slow electron flux, however, is zero in the CDS. Indeed, it is assumed that slow electrons are not present in this region because they would immediately be accelerated by the electric field and would not remain slow. However, their flux increases considerably in the NG, as more

and more fast electrons are slowed down by collisions and are transferred to the slow electron group. In the NG, most current is carried by the electrons, especially the slow ones. The Ar ion flux changes sign in this region; hence Ar ions will bombard the anode as well.

Figure 3e shows the mean energies of electrons, Cu ions, Ar ions, and fast Ar atoms as a function of distance from the cathode. The electrons (no. 1) start at the cathode with rather low energies and gain energy in the CDS because of the electric field. However, they also lose energy by collisions, so their mean energy at the CDS–NG interface is not equal to the discharge voltage but is about half of this value. The electron energy decreases in the NG because electrons do not gain energy from the electric field (which is very small) anymore, but they lose their energy more efficiently because of collisions. Farther in the NG, the electron energy remains more or less constant because the electrons travel back and forth in this region.

The Cu ions, Ar ions, and fast Ar atoms are thermalized in the NG, and their energy increases as they move toward the cathode. The mean Cu ion energy (no. 2) at the cathode is ~700 eV (about 70% of the discharge voltage), because the Cu ions do not lose their energy efficiently by collisions. Indeed, as was indicated in Figure 1, they are only subject to elastic collisions with Ar atoms; asymmetric charge transfer collisions with Ar atoms have a lower cross section, and symmetric charge transfer with Cu atoms is of low probability due to the much lower Cu atom density as compared with the Ar atom density (the latter is $\sim 10^{16}$ cm$^{-3}$).

The Ar ions (no. 3), however, reach a maximum mean energy of only ~150 eV (15% of the discharge voltage) at the cathode because these species lose the energy they gained from the electric field more efficiently as a result of symmetric charge transfer collisions with Ar atoms. The mean energy of the fast Ar atoms (no. 4) at the cathode is only ~30 eV (~3% of the discharge voltage). Indeed, these species are created from the Ar ions with energies corresponding to the Ar ion energies, but they cannot gain more energy from the electric field. It should be mentioned that the term "fast" Ar atoms is used for those atoms that are not thermalized and that have energies >0.05 eV.

From the energies and the fluxes of the species bombarding the cathode (i.e., Ar ions, fast Ar atoms, and Cu ions), the amount of sputtering can be calculated. It is generally found that the flux of fast Ar atoms bombarding the cathode is higher than the fluxes of Ar ions and Cu cathode ions. Therefore, the fast Ar atoms play a dominant role in sputtering. However, the efficiency of sputtering increases with the energy of the bombarding particles and with their mass (*34*); therefore, it is expected that the contribution of Cu cathode ions to sputtering (so-called self-sputtering) is nonnegligible, in spite of their lower total flux. It was calculated that the fast Ar atoms, Ar ions, and Cu cathode ions contribute ~70%, 25–30%, and 0.1–5% to the sputtering, respectively, at the typical discharge conditions used in GDMS.

*When applied to different cell geometries, models can predict plasma behavior and performance in analytical applications.*

Finally, Figures 3f and 3g show the ionization rates of Ar atoms and Cu atoms. The Ar atoms are ionized mainly by electron impact ionization, but fast Ar ion and atom impact ionization also play a role in the CDS, especially close to the cathode where the Ar ions and atoms reach their maximum energy (Figure 3e). Integrated over the entire discharge region, electron and fast Ar ion and atom impact ionization contribute ~90%, 2%, and 8%, respectively, to the ionization of Ar. A similar figure (not shown) would illustrate the excitation rate of Ar atoms, with a maximum adjacent to the cathode caused by fast Ar ion and atom impact excitation and a second peak in the beginning of the NG caused by electron impact excitation. This corresponds well to the luminous intensity throughout the GD. The NG is the most luminous part of the discharge, but close to the cathode, a bright layer, called the cathode glow, is often observed.

For the ionization of sputtered Cu atoms, Ar ion and atom impact ionization are not included in the model, basically because no cross sections are available in the literature. However, besides electron impact ionization, two other processes come into play for the sputtered atoms (i.e., Penning ionization by Ar metastable atoms and asymmetric charge transfer with Ar ions). Both of these processes seem to be more important than electron impact ionization. The relative contributions of Penning ionization, asymmetric charge transfer, and electron impact ionization, integrated over the entire discharge region, were calculated to be 60%, 36%, and 4%, respectively, at the discharge conditions of 1000 V and 3 mA. These values are only approximate because the rate coefficients of Penning ionization, and especially of asymmetric charge transfer, are subject to uncertainties. Moreover, these calculated contributions depend strongly on the discharge conditions, cell dimensions, and especially the type of sputtered material.

Although these results are interesting and allow us to obtain a better insight into GD, they are not of direct analytical importance. Nevertheless, the models we have developed can also be useful for better analytical practice. From the flux of sputtered cathode atoms and the flux of redeposition of these atoms back to the cathode (both as a function of radial distance), the crater profiles caused by sputtering at the cathode can be calculated, and they reflect the experimental crater profiles reasonably well (*28*). Therefore, the models can be used to predict the optimal discharge conditions and cell geometry to obtain flat crater bottoms, which are necessary for good depth resolution in depth-profiling analysis.

Furthermore, when the models are applied to different cell geometries, they can be used to predict trends in plasma behavior and performance in analytical applications, such as optimizing ion currents at the exit slit to the mass spectrometer. They can therefore be useful in new

cell design, for example, in investigating the influence of cell dimensions (*25*) and when comparing two cells with pin and flat cathodes (*26*).

Finally, because of the insight we acquired with our modeling work, we can explain differences in relative sensitivity factors (RSFs) in GDMS for a range of elements by an explicit treatment of the physical processes occurring in a GD. From a systematic study of 42 elements, we concluded that asymmetric charge transfer is responsible for the variations in RSFs, which could not be explained by transport phenomena and Penning ionization only (*32*). The limitation of this RSF model is that exact values for the rate coefficients of asymmetric charge transfer for various elements are not yet available in the literature. If these values could be measured with good accuracy, exact values of RSFs could be calculated and used for practical GDMS analysis.

## Summary

Our work in modeling an analytical dc GD in Ar has yielded satisfactory agreement between calculations and experimental observations, demonstrating that the models present a nearly realistic picture of the GD. Fundamental plasma quantities can be calculated for typical GDMS conditions. The models can also be used to predict crater profiles and sputtering rates at the cathode, optical emission spectra, ion fluxes entering the mass spectrometer, and variations in RSFs for GDMS. Therefore, they can be of direct analytical interest. Moreover, the modeling network can be applied to specific cell geometries, and it can provide information on trends in plasma conditions and application results. This can be useful in cell design.

In future work, we would like to extend the present models to other types of GDs, which are being used more and more for analytical applications such as rf-powered and pulsed GDs, magnetron-assisted discharges, and hyphenated types of discharges.

Mathematical modeling is a useful tool for obtaining better insight into the complexity of the GD. Experimental validation will always be necessary, but modeling can be complementary because it often provides information that is experimentally difficult to acquire.

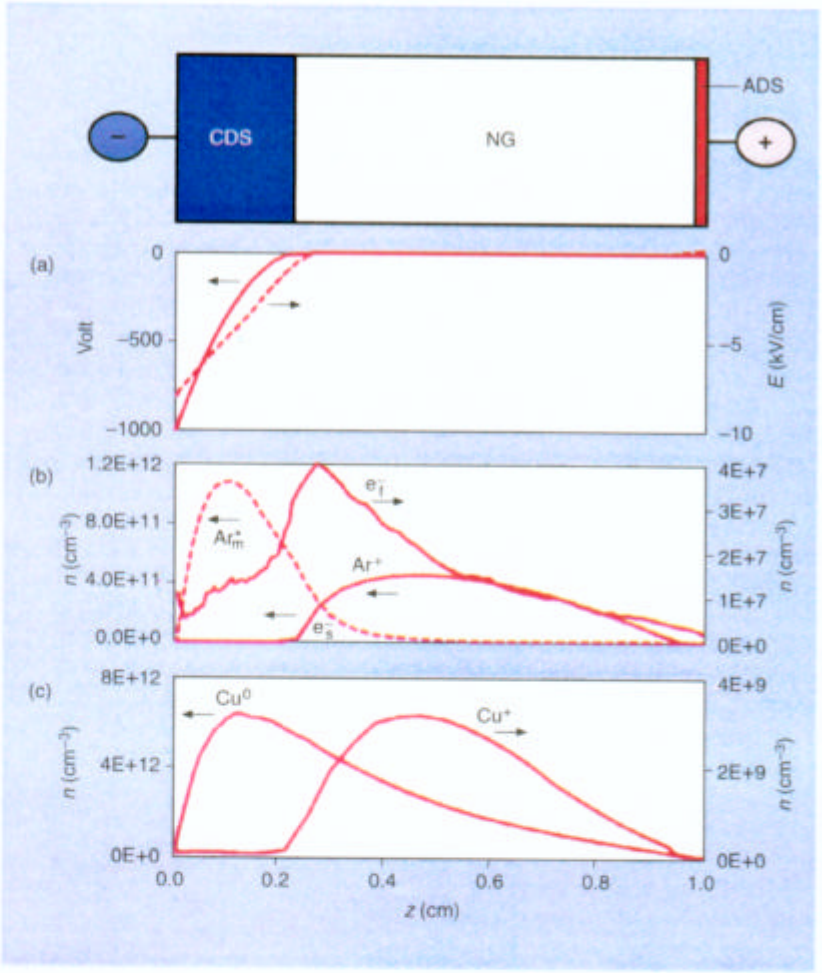


**Figure 3. Calculated characteristic plasma quantities in one dimension, as GDMS at 1000 V, 3 mA, and 75 Pa.**

(a) Potential and electric field distributions. (b) Number density profiles of Ar metastable atoms, ions. (d) Fluxes of Ar ions, fast and slow electrons, and total flux flowing through the discharge. discharge. (f) Ionization rates of Ar atoms (1, total; 2, by electrons; 3, by Ar ions; 4, by Ar atoms). 4, electron impact ionization).

A. Bogaerts wishes to acknowledge the Flemish Foundation for Scientific Research for financial support.

## References


(1) Harrison, W. W.; Hess K. R.; Marcus R. K.; King F. L. *Anal. Chem.* **1986**, *58*, 341 A.
(2) Harrison, W. W.; Barshick, C. M.; Klingler J. A.; Ratliff, P. H.; Mei Y. *Anal. Chem.* **1990**, *62*, 943 A.
(3) Marcus, R. K. *Glow Discharge Spectroscopies*; Plenum Press: New York, 1993.
(4) Chapman, B. *Glow Discharge Processes*; John Wiley & Sons: New York, 1988.
(5) Boeuf, J. P. *J. Appl. Phys.* **1988**, *63*, 1342.
(6) Meyyappan, M.; Govindan, T. R. *J. Appl. Phys.* **1993**, *74*, 2250.
(7) Passchier, J.D.P.; Goedheer, W. J. *J. Appl. Phys.* **1993**, *74*, 3744.
(8) Carman, R. J. *J. Phys. D: Appl. Phys.* **1989**, *22*, 55.
(9) Surendra, M.; Graves, D. B.; Jellum, G. M. *Phys. Rev. A: At., Mol., Opt. Phys.* **1990**, *41*, 1112.
(10) Weng, Y.; Kushner, M. *Phys. Rev. A: At., Mol., Opt. Phys.* **1990**, *42*, 6192.
(11) Donko, Z.; Rozsa, K.; Tobin, R. C. *J. Phys. D: Appl. Phys.* **1996**, *29*, 105.
(12) Bogaerts, A.; van Straaten, M.; Gijbels, R. *Spectrochim. Acta* **1995**, *50B*, 179.
(13) Bogaerts, A.; Gijbels, R.; Goedheer, W. J. *J. Appl. Phys.* **1995**, *78*, 2233.
(14) Bogaerts, A.; Gijbels, R. *J. Appl. Phys.* **1995**, *78*, 6427.
(15) Bogaerts, A.; Gijbels, R. *Phys. Rev. A: At., Mol., Opt. Phys.* **1995**, *52*, 3743.
(16) Bogaerts, A.; van Straaten, M.; Gijbels, R. *J. Appl. Phys.* **1995**, *77*, 1868.
(17) Bogaerts, A.; Gijbels, R. *J. Appl. Phys.* **1996**, *79*, 1279.
(18) Bogaerts, A.; Gijbels, R.; Goedheer, W. J. *Anal. Chem.* **1996**, *68*, 2296.
(19) Bogaerts, A.; Gijbels, R. *Anal. Chem.* **1996**, *68*, 2676.
(20) Bogaerts, A. Ph.D. dissertation, University of Antwerp, 1996.
(21) Bogaerts, A.; Gijbels, R.; Vlcek, J. *J. Appl. Phys.*, submitted.
(22) Aston, F. W. *Proc. Roy. Soc. London, Ser.*

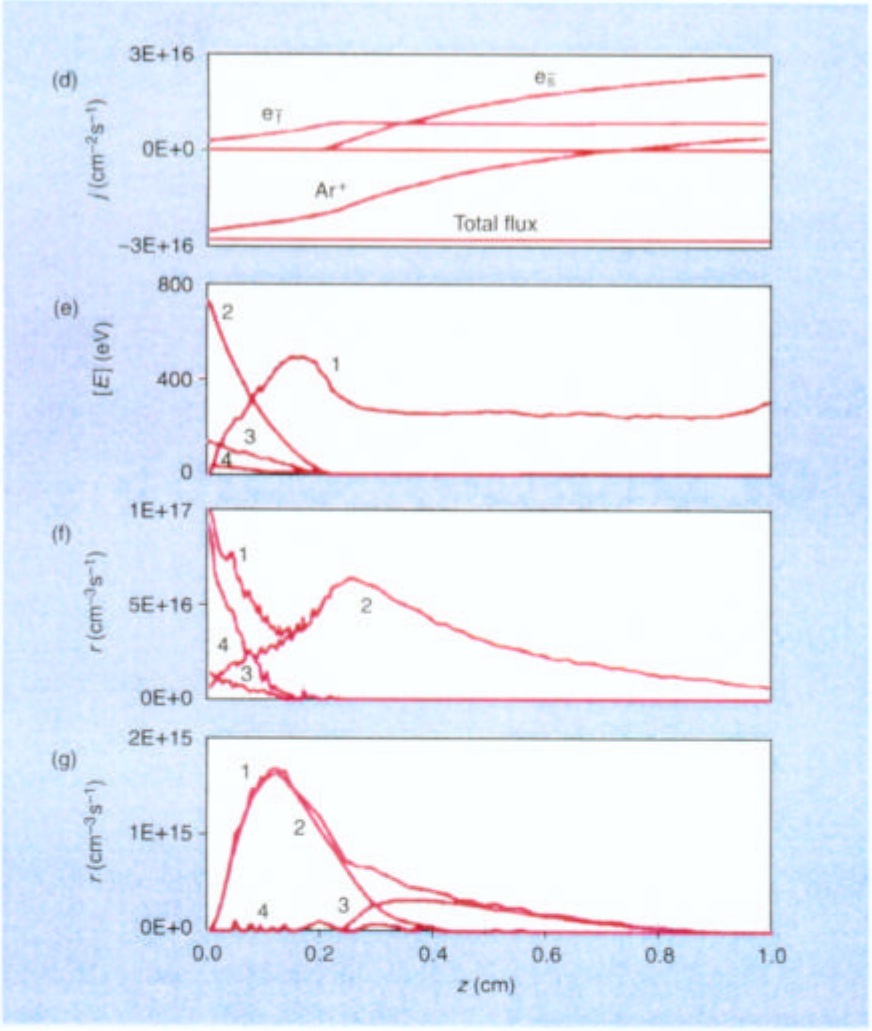


**a function of distance from the cathode, for a typical GD cell used in**

Ar ions, and slow and fast electrons. (c) Number density profiles of sputtered Cu atoms and Cu
(e) Mean energies of electrons (1), Cu ions (2), Ar ions (3), and fast Ar atoms (4) throughout the
(g) Ionization rates of Cu atoms (1, total; 2, Penning ionization; 3, asymmetric charge transfer;

*A* **1907**, *79*, 80.
(23) Bogaerts, A.; Guenard, R. D.; Smith, B. W.; Winefordner, J. D.; Harrison, W. W.; Gijbels, R. *Spectrochim. Acta* **1997**, *52B*, 219.
(24) Bogaerts, A.; Wagner, E.; Smith, B. W.; Winefordner, J. D.; Pollmann, D.; Harrison, W. W.; Gijbels, R. *Spectrochim. Acta* **1997**, *52B*, 205.
(25) Bogaerts, A.; Gijbels, R. *J. Anal. At. Spectrom.* **1997**, *12*, 751.
(26) Bogaerts, A.; Gijbels, R. *J. Am. Soc. Mass Spectrom.* **1997**, *8*, 1021.
(27) van Straaten, M.; Bogaerts, A.; Gijbels, R. *Spectrochim. Acta* **1995**, *50B*, 583.
(28) Bogaerts, A.; Gijbels, R. *Spectrochim. Acta* **1997**, *52B*, 765.
(29) Jonkers, C. Ph.D. dissertation, University of Antwerp, 1995.
(30) Dwight, E.; Billings, B. H.; Bleil, D. F. *American Institute of Physics Handbook*, 3rd Edition; McGraw-Hill: New York, 1972.
(31) Rozsa, K; Gallagher, A.; Donko, Z. *Phys. Rev. E: Stat. Phys., Plasmas, Fluids, Relat. Interdiscip. Top.* **1995**, *52*, 913.
(32) Bogaerts, A.; Gijbels, R. *J. Anal. At. Spectrom.* **1996**, *11*, 841.
(33) Vieth, W.; Huneke, J. C. *Spectrochim. Acta, Part B* **1991**, *46*, 137.
(34) Matsunami, N. et al. *Atomic Data Nucl. Data Tables* **1984**, *31*, 1.

*Annemie Bogaerts is a postdoctoral researcher at the University of Antwerp. Her research focuses on the fundamental study of glow discharges for analytical and technical applications. Renaat Gijbels is professor of physical chemistry and co-director of the Micro and Trace Analysis Center. His research focuses on solids MS and electron, ion, and laser microbeam techniques for trace, surface, and microanalyses. Address correspondence about this article to Bogaerts, Department of Chemistry, University of Antwerp, Universiteitsplein 1, B-2610, Wilrijk-Antwerp, Belgium (bogaerts@uia.ua.ac.be).*